

Article

Phosphate Removal by Ca-Modified Magnetic Sludge Biochar Prepared by a One-Step Hydrothermal Method

Xu Liu ¹, Yushan Li ^{1,*}, Hao Zhou ^{2,*} , Jing Guo ³, Yonghou Xiao ¹, Cong Liu ⁴, Boxing An ¹ and Zhengqi Liang ¹

¹ Liaoning Key Laboratory of Chemical Additive Synthesis and Separation, Panjin Institute of Industrial Technology, Dalian University of Technology, Panjin 124221, China; xu_liu@dlut.edu.cn (X.L.); yonghou.xiao@dlut.edu.cn (Y.X.); anboxing123@163.com (B.A.); liangzhengqi521@163.com (Z.L.)

² School of Ocean Science and Technology, Dalian University of Technology, Panjin 124221, China

³ School of Chemical Engineering, Panjin Campus, Dalian University of Technology, Panjin 124221, China; 15265188264@163.com

⁴ Shandong HELP Safety and Environmental Protection Technique Pty Ltd., Panjin Branch, Panjin 124221, China; lc04060223@163.com

* Correspondence: liyushan@dlut.edu.cn (Y.L.); zhouhao@dlut.edu.cn (H.Z.)

Abstract: The problem of phosphorus pollution and its resource utilization has been a source of general concern. The preparation of green, renewable, and non-secondary pollution adsorbents has become a research direction. In this paper, a one-step hydrothermal preparation method of Ca-modified magnetic sludge biochar (Ca-MSBC) is used for enhancing phosphate removal. The results show that the adsorption rate of phosphate by Ca-MSBC is mainly controlled by chemisorption but is also related to physical adsorption and an internal diffusion mechanism. The maximum phosphorus adsorption capacity of Ca-MSBC was 89.25 mg g⁻¹ at 343 K (initial phosphate concentration 500 mg L⁻¹). After nine cycles of adsorption experiments, the adsorption capacity of 70.16 mg g⁻¹ was still high. In addition, coexisting ions Cl⁻, NO₃⁻, SO₄²⁻, and CO₃²⁻ have no significant effect on the adsorption properties of phosphate. XRD, FT-IR, VSM, XPS, and N₂ adsorption/desorption isotherms showed that the mechanism of phosphate removal from water by Ca-MSBC was mainly the chemical precipitation reaction of phosphate and calcium. The results of this study indicate that Ca-MSBC has potential application and environmental value as a solid waste recycling material for environmental remediation.

Keywords: calcium; magnetic biochar; phosphate; resource reuse; sewage sludge



Citation: Liu, X.; Li, Y.; Zhou, H.; Guo, J.; Xiao, Y.; Liu, C.; An, B.; Liang, Z. Phosphate Removal by Ca-Modified Magnetic Sludge Biochar Prepared by a One-Step Hydrothermal Method. *Catalysts* **2023**, *13*, 927. <https://doi.org/10.3390/catal13060927>

Academic Editors: Zichuan Ma and Xing Zhou

Received: 24 April 2023

Revised: 20 May 2023

Accepted: 21 May 2023

Published: 24 May 2023



Copyright: © 2023 by the authors. Licensee MDPI, Basel, Switzerland. This article is an open access article distributed under the terms and conditions of the Creative Commons Attribution (CC BY) license (<https://creativecommons.org/licenses/by/4.0/>).

1. Introduction

With the continuous improvement of the economic level, the population has been rapidly increasing. The world's population is expected to reach 10.1 billion in 2050 [1]. Population growth is associated with increases in wastewater discharge, and phosphate is one of the main pollutants in the wastewater treatment process. With the increasing use of household washing products and agricultural fertilizers, more and more P is discharged into environmental water. The increase in phosphate concentration in water will cause eutrophication, leading to water pollution. In addition, phosphate resources are decreasing worldwide, and the demand for phosphate in agriculture and forestry is increasing year by year [2–8], resulting in a prominent contradiction between phosphate emissions and phosphate demand. With the increase in wastewater production, the sewage sludge (SS) produced by wastewater treatment plants is also increasing year by year. According to statistics, the SS produced in the sewage treatment process in China is about 20 million tons (dry base) every year, and if a large amount of SS is not properly disposed of, it will cause serious harm to the environment [9]. In addition, SS contains about 10–20 g kg⁻¹ of phosphorus resources, and the conventional landfill disposal of SS occupies land while preventing the phosphorus resources from being recycled. Therefore, how to safely treat

SS and recover P from wastewater and sludge to achieve the recycling of SS resources has become a hot research topic in recent years.

At present, the removal methods of phosphate pollutants in the process of sewage treatment mainly include chemical precipitation and biochemical and adsorption methods. The chemical and biochemical methods have the problems of multi-factor constraints, large sludge production, high operating cost, and difficult process control. By contrast, the adsorption method is considered a promising phosphorus removal technology due to its advantages of low cost, high selectivity, and simple operation [10]. Adsorption materials are generally divided into natural materials, waste materials, and synthetic materials. For example, natural materials such as walnut shell [11,12], struvite [13,14], agricultural waste straw [15,16], and synthetic materials such as (Fe-Al-MOF) [17,18] have been reported continuously in recent years. However, most of the adsorption materials have disadvantages such as high raw material cost, low adsorption efficiency and capacity, poor regeneration capacity, and poor performance stability [19,20]. Compared with other adsorption materials, SS has the advantages of wide source, high carbon content (17–23%), and rich functional groups (C-O-C, C=O-, -CH₃, -CH₂-) [21,22]. At the same time, SS has attracted wide interest because of its low cost and environmentally friendly characteristics [23,24].

In recent years, the research on sludge source adsorption materials has focused on the removal of organic pollutants and heavy metals [25–28]. Scholars in the field have also carried out a series of studies on the removal of phosphate from sewage by SS biochar. Peng et al. [29] prepared Mn/Al modified sludge biochar by a one-step hydrothermal method, and the maximum phosphate adsorption capacity of phosphate at 298 K was 28.20 mg g⁻¹. Zhang et al. [30] prepared SS biochar by pyrolysis and found that mineral particles containing Si, Ca, Al, and Fe formed the active site of phosphate binding on the surface of sludge biochar, among which minerals containing calcium played a major role in removing phosphate. As a strong magnetic material, Fe₃O₄ is conducive to the recycling of biochar. Additionally, the incorporation of the Fe element will further increase the adsorption sites of biochar and enhance its adsorption capacity for phosphate. At present, there is a lack of research on the regulation effects of Fe and Ca bimetals on the pore size of SS biochar adsorption materials and the mechanism and process parameters of phosphate adsorption.

In this paper, Ca-modified sludge-sourced magnetic carbon (Ca-MSBC) with a mesoporous structure was synthesized by a simple and green one-step hydrothermal method for the removal of phosphate pollutants from wastewater. The five components of this study were as follows: (1) the structure and composition of the prepared Ca-MSBC were characterized using scanning electron microscopy (SEM), X-ray diffraction (XRD), Fourier transform infrared spectroscopy (FT-IR), vibrating sample magnetometer (VSM), and N₂ adsorption/desorption isotherms; (2) magnetic material (Fe₃O₄) was introduced to realize the rapid separation and recycling of the adsorbent; (3) the adsorption efficiency of Ca-MSBC to phosphate in wastewater was investigated under different operating environments (pH, temperature, time, and coexisting ions); (4) through the analysis of adsorption kinetics, the adsorption mechanism of phosphate by Ca-MSBC was elaborated; (5) The application potential of Ca-MSBC in real wastewater was evaluated. Our ultimate goal is to use sewage sludge to develop a new material that is easy to recycle, can efficiently adsorb phosphate from wastewater, and has a wide range of applications.

2. Results and Discussion

2.1. Characterization of Ca-MSBC

Ca-MSBC adsorbents prepared with different molar concentrations of Ca were expressed as Ca-MSBC-Cax ($x = 0.02, 0.04, 0.06, 0.08, \text{ and } 0.10 \text{ mol}$). Figure 1A XRD shows that the characteristic peaks of Fe₃O₄ appear around 30.31°, 35.45°, 43.23°, 57.25°, 62.98°, and 74.53° (PDF#01-1111) [31] of Ca-MSBC-Cax. This indicates that Fe₃O₄ was successfully loaded onto the surface of the carbon matrix. In addition, Ca-MSBC-Cax showed characteristic peaks of CaO at 31.77°, 37.41°, and 68.45° (PDF#99-0070) [32]. This indicates that

calcium was successfully loaded onto the surface of Ca-MSBC and mainly exists in the form of CaO.

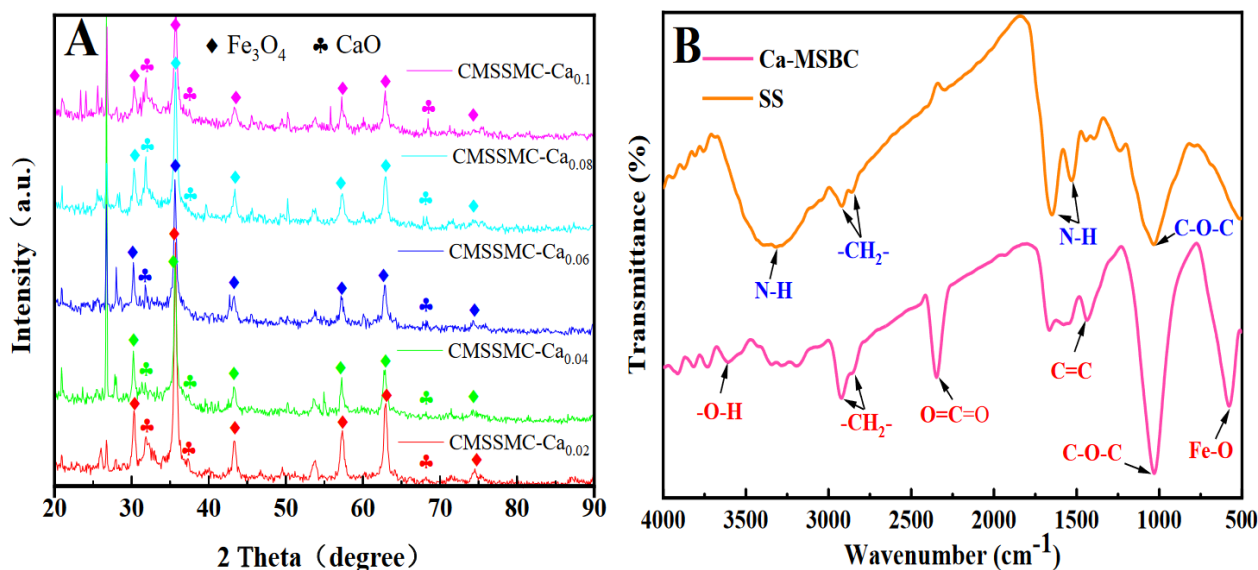


Figure 1. XRD (A) and FT-IR (B) patterns of Ca-MSBC.

As shown in Figure 1B, the characteristic peak of the Fe–O bond appeared at 575 cm^{-1} , indicating that Fe_3O_4 was successfully magnetized on Ca-MSBC [33]. Meanwhile, 1032 cm^{-1} is the C–O–C characteristic peak, 1432 cm^{-1} is the C=C characteristic peak, and 3604 cm^{-1} is the -O–H characteristic peak. In addition, the C–O–C characteristic peak at 1032 cm^{-1} was significantly enhanced compared with SS, which indicated that the magnetization and calcium modification of Ca-MSBC could form the active site.

SS and Ca-MSBC were characterized by EDX. Compared with SS, the atomic percentage of Fe and Ca increased by 3.68% and 0.36% in Ca-MSBC, which further proved the successful loading of iron and calcium ions in Ca-MSBC.

As shown in Figure 2A, the structure of activated sludge is dispersed, and the surface is relatively smooth. Figure 2B shows that the channels and holes of Ca-MSBC provide a large specific surface area. Combined with the analysis results in Table S1 and Figure 1, it is proved that Fe_3O_4 and CaO are successfully loaded on the surface of carbon-based carriers. The large specific surface area and large number of active sites of Ca-MSBC are helpful for improving the adsorption performance of Ca-MSBC for phosphate [34].

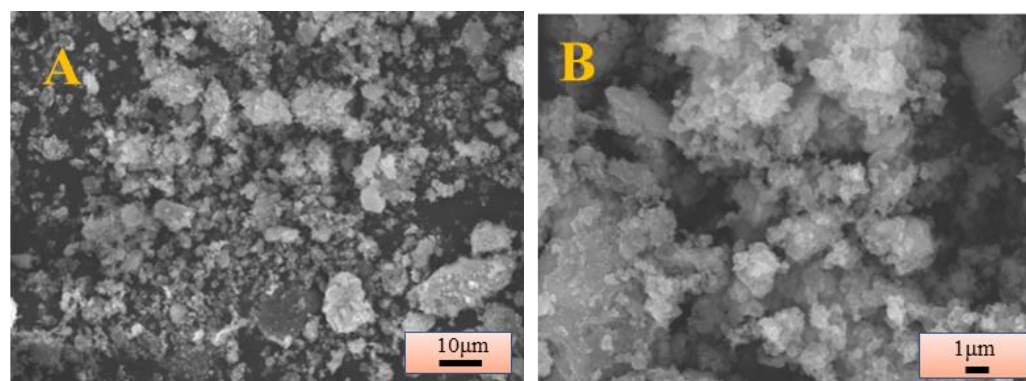


Figure 2. Cont.

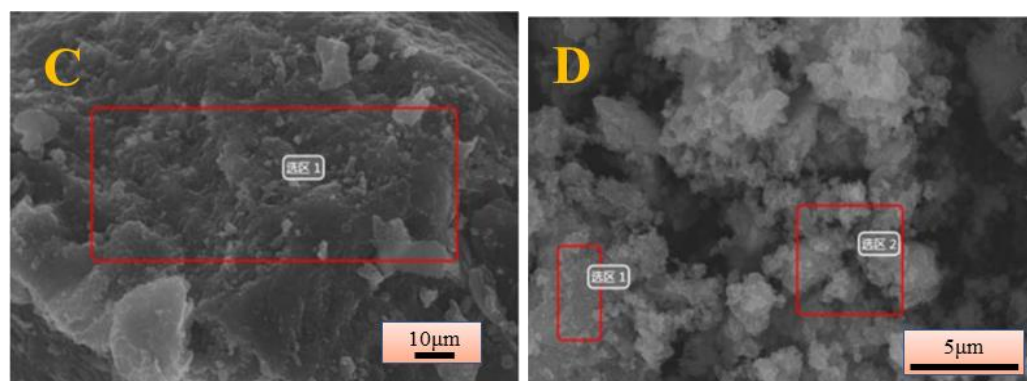


Figure 2. SEM and EDX (A,C) of SS; SEM and EDX (B,D) of Ca-MSBC. The Chinese term showed in (C,D) means region.

The possible adsorption mechanism was explored by characterizing the Ca-MSBC before and after phosphate adsorption by XPS spectroscopy. As seen in Figure 3A, the Ca-MSBC adsorbent is mainly composed of C, O, Fe, Ca, and P elements. In Figure 3D phosphate produces a P 2p peak at ~ 133.4 eV, demonstrating that phosphate is successfully adsorbed, moving toward the lower energy side compared to the pure KH_2PO_4 adsorbent (133.7 eV); the P 2p peak shifted to a lower energy, indicating that phosphate and Ca-MSBC were tightly bound by chemical bonds [35]. Figure 3A,B,D show that the O 1s binding energy of 531.4 eV, Ca $2p_{2/3}$ 347.3 eV, and P 2p 133.4 eV indicate that phosphate could be adsorbed on the surface of Ca-MSBC in the form of CaHPO_4 , while Ca-MSBC has a good adsorption effect on phosphate under alkaline conditions. It has been reported that phosphate at effluent $7.0 < \text{pH} < 10.0$ is mainly in the form of HPO_4^{2-} , which further supports the above conclusion.

VSM can verify the magnetization intensity of Ca-MSBC, which is an important performance index of magnetic materials. As can be seen in Figure 4, the SS hysteresis line is almost straight, and in comparison, Ca-MSBC shows an S-shaped hysteresis loop, which indicates that the material shows ferrimagnetic behavior [36]. The Ca-MSBC saturation magnetization was 0.18 emu g^{-1} , the value of coercivity was 55.46 Oe, and remanence was 0.02 emu g^{-1} [37,38]. In addition, Ca-MSBC is easily adsorbed by magnets, which is conducive to the magnetic separation of Ca-MSBC for recovery and reuse [39].

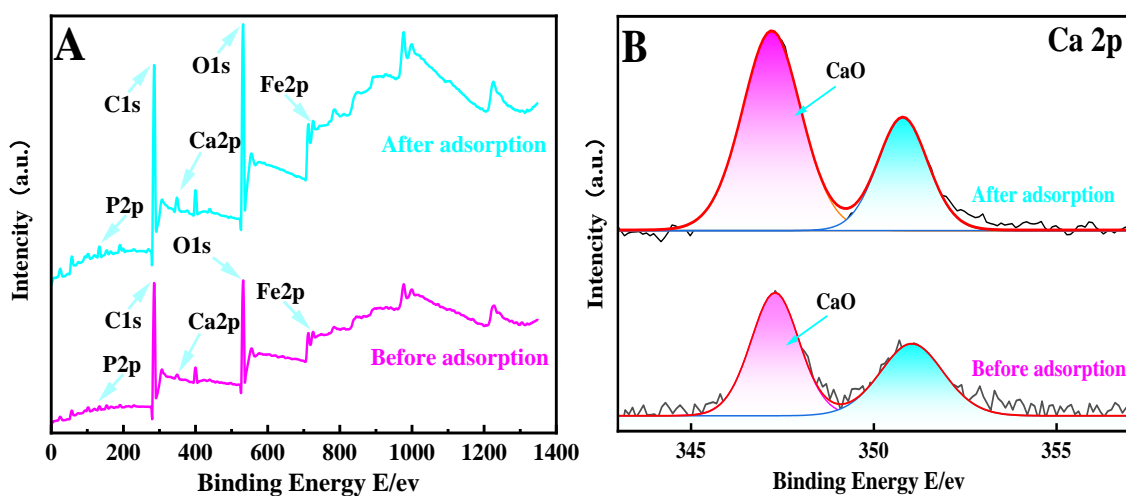


Figure 3. Cont.

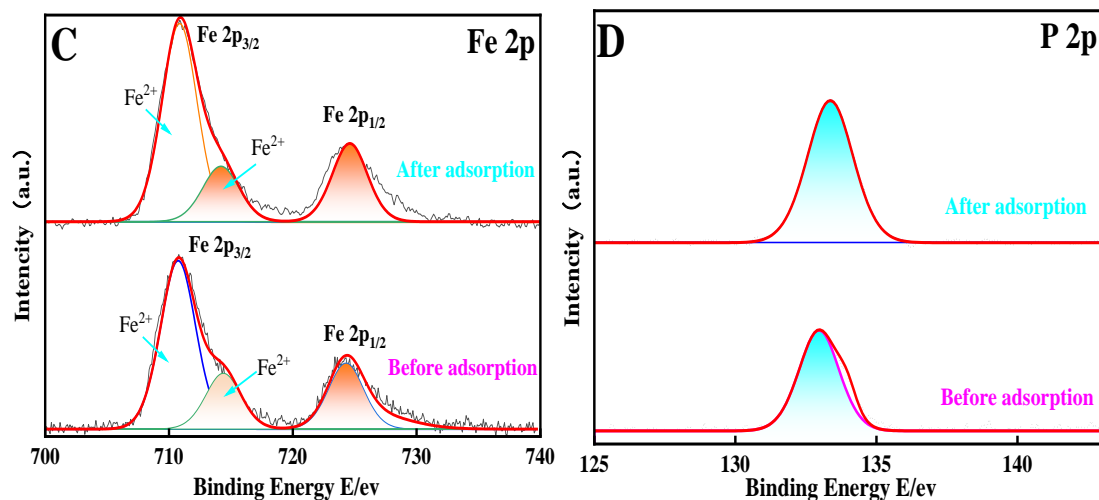


Figure 3. XPS analysis of Ca-MSBC before and after phosphate adsorption: (A) XPS full survey spectra (B), Ca 2p spectra, (C) Fe 2p spectra, and (D) P 2p spectra.

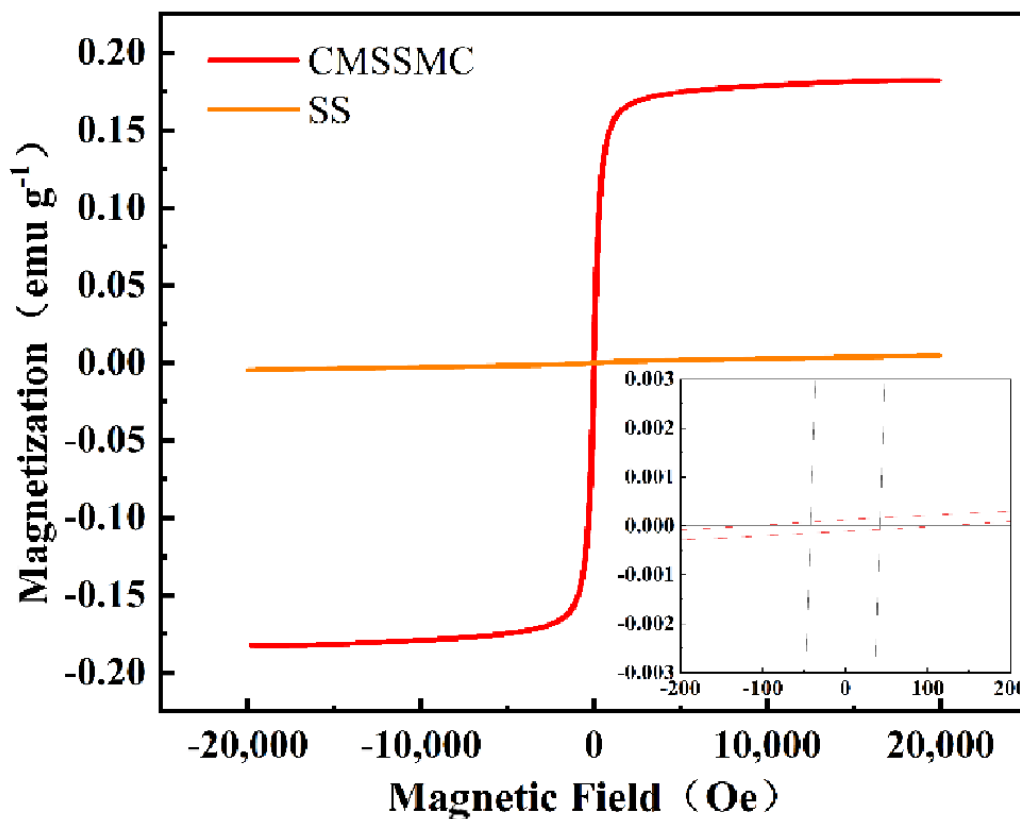


Figure 4. SS and Ca-MSBC magnetization curve.

The pore structure of Ca-MSBC was characterized by N_2 adsorption/desorption isotherms, and the effect of phosphate adsorption on pore structure was analyzed. As shown in Figure 5A, N_2 adsorption and desorption isotherms of magnetic carbon samples before and after Ca-MSBC adsorption belong to typical type IV isotherms, which shows that Ca-MSBC adsorbent has a typical mesoporous structure [40]. At $p/p_0 = 0.6\sim 1.0$, the adsorption isotherms and desorption isotherms gradually separate with the increase of p/p_0 , and the H4-type hysteresis loop is generated, further proving the existence of the mesoporous structure of Ca-MSBC.

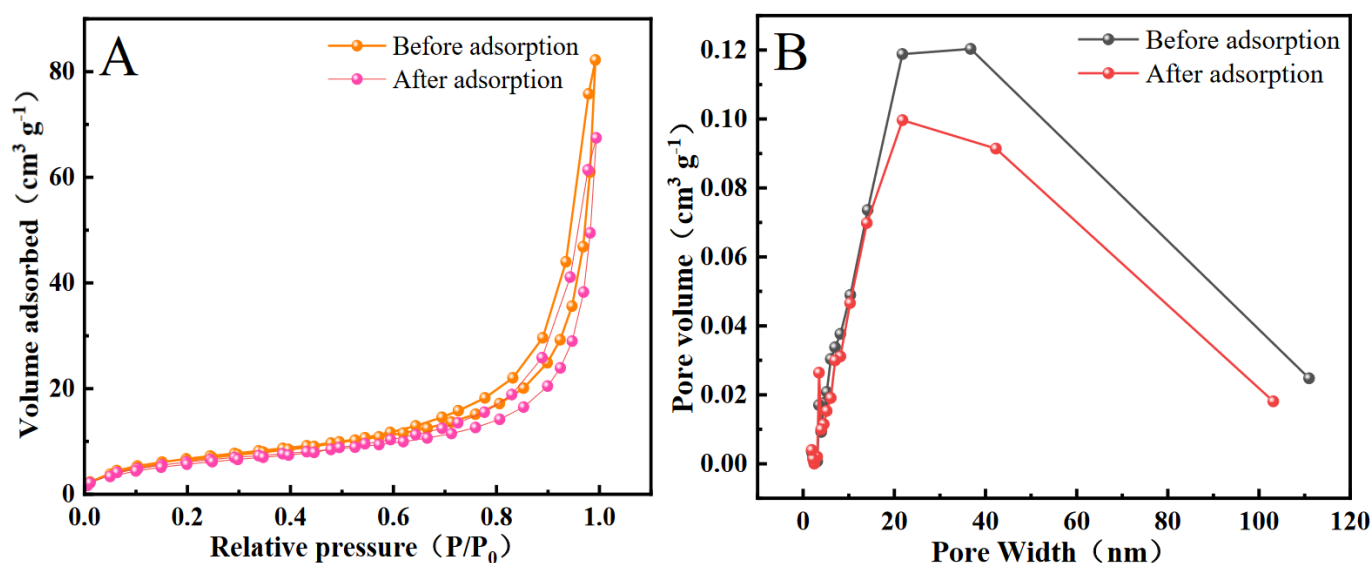


Figure 5. Adsorption and desorption isotherms and pore size distribution curves of samples before and after Ca-MSBC adsorption. (A) Nitrogen adsorption–desorption isotherms; (B) Pore size distribution.

As shown in Figure 5B, the pore size of Ca-MSBC before and after adsorption is mainly distributed between 20 and 40 nm, and Table S2 shows that the average pore size is 18–19 nm, which proves again that Ca-MSBC is dominated by a mesoporous structure. At the same time, it was found that the total surface area, total pore volume, and average pore size of Ca-MSBC decreased to different degrees after adsorbing phosphate, which may be related to phosphate occupying the adsorption site of Ca-MSBC.

2.2. Effect of Adsorption Conditions on the Phosphorus Removal Performance of Ca-MSBC

Research shows that the main form of phosphate under different pH values is as follows: H_3PO_4 (pH < 2.16), H_2PO_4^- (pH = 2.16–7.21), HPO_4^{2-} (pH = 7.21–12.31), and PO_4^{3-} (pH > 12.32) [41]. Figure 6A showed that the adsorption capacity of Ca-MSBC for phosphate changed significantly with the increase in pH value. Under acidic conditions, phosphate substances mainly exist in water in the form of HPO_4^{2-} and cannot react with Ca^{2+} to form precipitation, so the removal efficiency is low. At the same time, Table S1 shows that Ca-MSBC contains a certain amount of phosphorus element, and under acidic conditions, phosphate on the surface of Ca-MSBC is dissolved and released into the water. As a result, the phosphate adsorption capacity is negative. Similar experimental results and inferences have also been mentioned in the relevant literature [42]. Phosphate with $7.0 < \text{pH} < 10.0$ exists in the form of HPO_4^{2-} . CaHPO_4 (2.57×10^{-7}) [43] and $\text{Ca}_5(\text{PO}_4)_3(\text{OH})$ (3.7×10^{-58}) have low k_{sp} values [44]. Therefore, HPO_4^{2-} tends to react with Ca^{2+} and precipitate on the surface of the prepared adsorbent. At the same time, the surface of Ca-MSBC is positively charged due to the proton-carrying positive charge of the Me-OH group, which promotes the electrostatic attraction between phosphate anions [45,46]. These two points are conducive to the adsorption of phosphate by Ca-MSBC. Therefore, when the pH value is 9.0, the phosphate adsorption capacity reaches 43.2 mg g^{-1} . When the pH value was further increased to 10.0, the phosphate adsorption capacity decreased by 0.4 mg g^{-1} to a certain extent. The reason is that the negative charge generated on the surface due to the deprotonation of Ca-MSBC in the strong alkali medium and the electrostatic repulsion between the phosphate anions resulted in a small decrease in the phosphate adsorption capacity [47]. Comparing the results of the S3 study, the adsorbent showed superior phosphate adsorption capacity under alkaline conditions compared to other similar biomass-derived biochar [48–51].

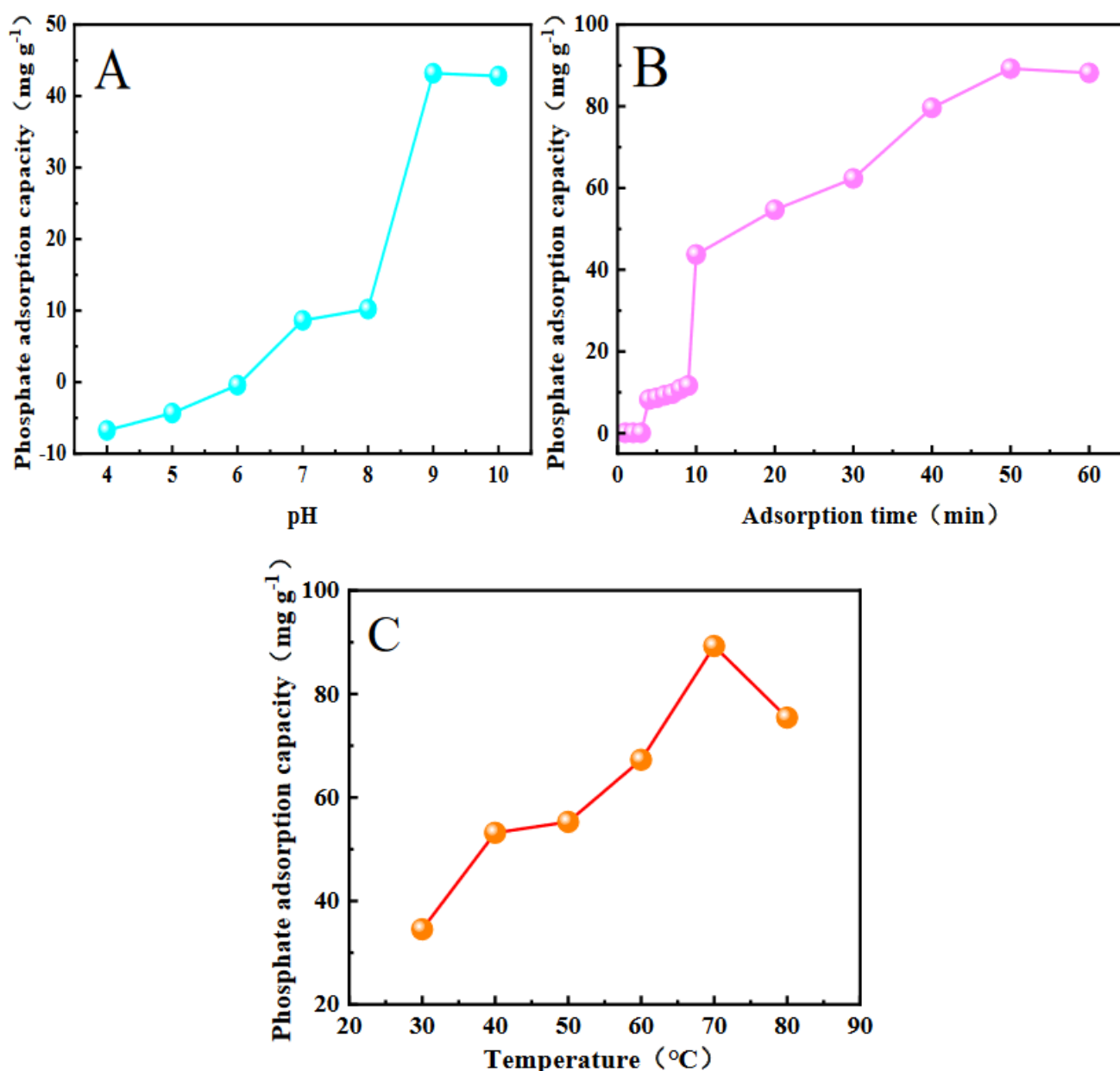


Figure 6. Effect of adsorption conditions on the phosphate adsorption performance of Ca-MSBC. (A) Effect of pH, (B) Effect of adsorption time, (C) Effect of temperature.

As shown in Figure 6B, when the adsorption time is 0–10 min, the adsorption rate is fast, and when the adsorption time is 10–60 min, the effect on Ca-MSBC's adsorption of phosphate is not obvious. The reason is that in the early stage of adsorption, the concentration difference between Ca-MSBC and phosphate in the solution is the largest, and the adsorption rate of phosphate by Ca-MSBC is positively correlated with the concentration difference. The larger the concentration difference, the easier it is for phosphate to overcome the mass transfer resistance and occupy the adsorption site, which is consistent with the research conclusion of Dong et al. [52]. The Ca-MSBC prepared in this experiment has a fast adsorption rate of phosphate at 0–10 min. Thus, the Ca-MSBC reached equilibrium very quickly after the onset of the reaction.

It is generally believed that in the process of phosphate adsorption, the amount of phosphate adsorption will increase with the increase in the solution temperature, which is related to the finding that an increase in temperature will increase the initial adsorption rate of phosphate adsorption and shorten the time needed for phosphate adsorption to reach

equilibrium [53]. At the same time, it was also reported that the increase in temperature increased the thermal energy of the system, increased the fluidity of phosphate ions, and promoted the occurrence of the adsorption process [54]. As shown in Figure 6C, the adsorption capacity gradually increases with the increase in temperature, because the adsorption process is an exothermic reaction process, and the increase in temperature is conducive to the improvement in adsorption efficiency. When the temperature exceeds 70 °C, phosphate adsorption capacity reaches adsorption equilibrium, and the tendency of phosphate molecules to increase their activity on the adsorbent surface leads to a decrease in adsorption efficiency.

2.3. Kinetics of Adsorption

As shown in Figure 7A, adsorption kinetics fitting of Ca-MSBC was carried out. According to the fitting results of the three kinetic models, the correlation coefficient of the pseudo-second-order kinetic model ($R^2 = 0.9899$) was higher than that of the pseudo-first-order kinetic model ($R^2 = 0.9742$). Moreover, this study found that if intraparticle diffusion is the only limiting step, the curve between q_e and $t^{0.5}$ must pass through the origin [55]. Figure 7B shows that although intraparticle diffusion is involved in the adsorption process, it is not the only control step, which further indicated that the mechanism of phosphate adsorption onto Ca-MSBC was not unique, but rather a reaction with several mechanisms. In the first stage of the adsorption reaction ($k_1 = 39.94$), the active center of Ca-MSBC enhanced the adsorption of phosphorus, and the main factor limiting the adsorption rate was membrane diffusion. In the second stage, the adsorption sites on the surface of Ca-MSBC were gradually saturated, resulting in the boundary layer. Therefore, the adsorption rate was decreased ($k_2 = 13.52$), and the adsorption process may be controlled by both in-particle diffusion and surface adsorption. In the third stage, the adsorption equilibrium stage was reached, and the adsorption rate of Ca-MSBC decreased significantly.

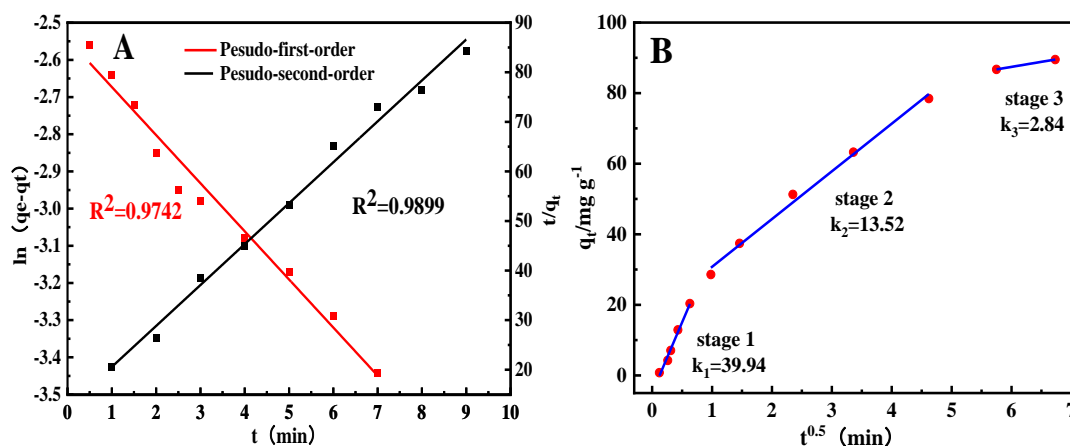


Figure 7. Kinetics of phosphorus adsorption on Ca-MSBC: (A) pseudo-first-order and pseudo-second-order; (B) intraparticle diffusion. (Initial P concentration was 500 mg L⁻¹ and the dosage of Ca-MSBC was 0.1 g L⁻¹).

2.4. Thermodynamics of Adsorption

The positive value of ΔH (S4) indicates that the adsorption of phosphate on Ca-MSBC is heat-absorbing, which is consistent with the previous results of increased adsorption efficiency at increasing temperatures. The positive value of ΔS indicates that the increase in disorder at the solid–liquid interface favors adsorption. In general, the adsorption process of P on Ca-MSBC is spontaneous and does not require additional external energy input, since $\Delta G < 0$ regardless of temperature. In addition, the magnitude of ΔG increases (becomes more negative) with increasing temperature, indicating that adsorption increases with temperature [56].

2.5. Effect of Coexisting Ions and the Reusability of Ca-MSBC

In order to analyze the effect of coexisting ions in wastewater on phosphate adsorption, the influence of anions such as Cl^- , NO_3^- , SO_4^{2-} , and CO_3^{2-} on phosphate adsorption was investigated under different conditions, as shown in Figure 8A. It can be observed that Cl^- has almost no effect on phosphate removal, and it is worth noting that NO_3^- can slightly increase phosphate removal, as shown by [57], a result that we confirmed was not due to measurement errors. Further studies will be conducted in future work. SO_4^{2-} has a slight effect on the adsorption performance, which may be related to the Helfferich anion exchange selectivity sequence. Compared with low-valence anions, high-valence anions are more likely to combine with Ca-MSBC adsorbents [58,59]. SO_4^{2-} reduces the adsorption capacity of the adsorbent for phosphates by competing for adsorption sites. Compared with other anions, CO_3^{2-} has a relatively large impact on phosphate adsorption, which may be due to the alkaline environment of the CO_3^{2-} solution, which reduces the adsorption capacity of the adsorbent [60].

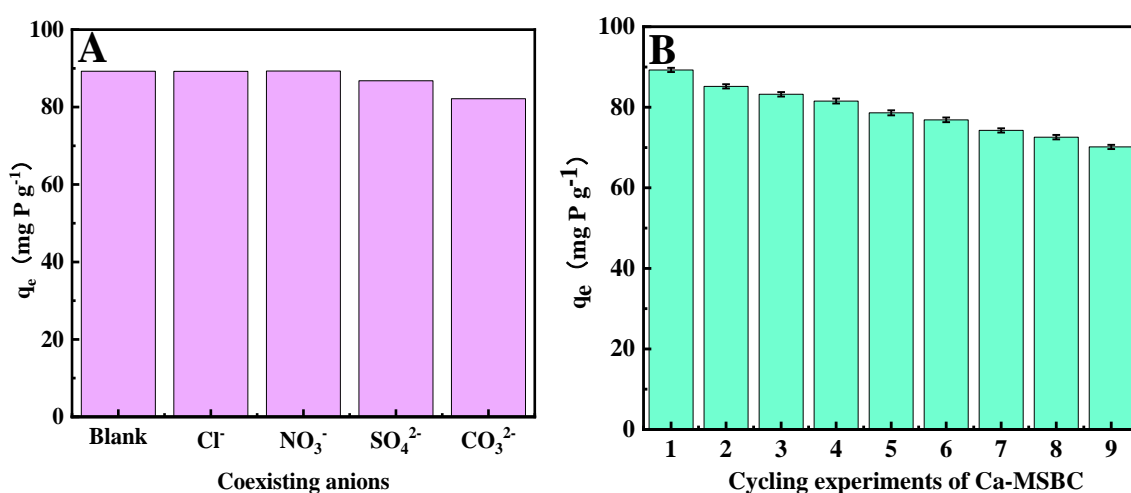


Figure 8. (A) Effect of coexisting anions on phosphate adsorption properties; (B) cycling experiments of Ca-MSBC.

In view of the great significance of adsorbent recovery for industrial applications, this experiment used a 0.1 M NaOH solution for the desorption of phosphate. The desorption process resulted in the desorption of phosphate from the adsorbent due to the formation of soluble Na_3PO_4 for the purpose of desorption. The results are shown in Figure 8B. Ca-MSBC still had a high adsorption capacity ($70.16 \text{ mg P g}^{-1}$) for phosphate after 9 consecutive adsorption–desorption cycles. There are two possible reasons for this. First, the decrease in adsorption capacity was related to the low desorption efficiency, which was caused by the low concentration of NaOH used for desorption, resulting in some phosphate not being completely desorbed from the adsorbent and occupying some of the active sites, and accumulating several times. Secondly, the CaO on the adsorbent surface may have been partially eluted during the elution process, resulting in fewer adsorption sites and reduced adsorption capacity. These results indicate that Ca-MSBC has good reusability.

It is worth mentioning that based on the above study results, we used the actual wastewater of a municipal sewage treatment plant to carry out the experiment on the adsorption effect of Ca-MSBC phosphorus. The phosphorus content at the inlet of the wastewater was 4.0 mg P L^{-1} , and adding 0.1 g of adsorbent, the phosphorus content in the effluent after adsorption was $<0.5 \text{ mg P L}^{-1}$, as required by the national discharge standard, proving that Ca-MSBC has a good adsorption effect on phosphorus in the actual wastewater treatment process, and has good prospects for industrial application.

3. Materials and Methods

3.1. Materials

All chemicals used in this study were analytical grade and used without further purification. FeCl_3 , $\text{FeSO}_4 \cdot 7\text{H}_2\text{O}$, CaCl_2 , and KH_2PO_4 were obtained from Shanghai Macklin Biochemical Co., Ltd., Shanghai, China. SS (dried sample) was produced from wet sludge released from the dewatering process at the Panjin wastewater treatment plant (Panjin, China) by drying at 105°C for 6 h, and the actual sewage comes from the inlet of the equalization tank at the same plant.

3.2. Preparation Method of Ca-MSBC

First, 50 mL of deionized water was added to a 100 mL glass bottle with a lid and stirred on a magnetic stirrer. FeCl_3 and $\text{FeSO}_4 \cdot 7\text{H}_2\text{O}$ were weighed according to $n_{\text{Fe}^{3+}} : n_{\text{Fe}^{2+}} = 1.5:1.0$. After being completely dissolved, 10 g SS was added, and the lid was tightened and stirred for 1 h. The pH was adjusted to 11.0 using a configured 10 mol L^{-1} NaOH solution, after which $n_{\text{Ca}} = 0.1\text{ mol}$ was added, and the mixture was stirred to fully dissolve and mix evenly with the sludge. The mixed solution was transferred to the hydrothermal reactor and reacted for 24 h at 180°C . After the hydrothermal reaction, magnetic biochar was separated with magnets and washed repeatedly with deionized water until the cleaning solution appeared clear, and then the magnetic biochar was placed in a drying oven at 100°C to prepare Ca-MSBC.

The water content of sewage sludge is about 80%, and water has a large heat capacity, so the hydrothermal method can reduce the heat loss, and make the pore size structure of the prepared material more uniform, which has a positive effect on improving the adsorption efficiency of Ca-MSBC. Hydrothermal carbonization temperature is usually between $150\text{--}280^\circ\text{C}$. Relevant studies have shown that the carbon conversion rate is highest at the hydrothermal reaction temperature of 180°C when the pH of the hydrothermal reaction is adjusted by NaOH, and the increase in hydrothermal time is beneficial to the homogeneous loading of metal oxides. Therefore, the above parameters were chosen as the hydrothermal synthesis conditions [61].

3.3. Method of the Static Adsorption Experiment

3.3.1. Static Adsorption Experiment

The initial pH of the solution was adjusted to 10.0 utilizing 1 M NaOH. Amounts of 0.1 g Ca-MSBC and 25 mL of KH_2PO_4 simulated water containing 500 mg L^{-1} were added, and stirred in a constant temperature oscillator at 30 r min^{-1} for 10 min. Considering the economics of the filtration process in industrial applications, this study used quantitative filter paper to simulate the filtration process for solid–liquid separation after adsorption and to determine the P content of the filtrate.

The wastewater used in the static adsorption test was obtained from the influent of the anaerobic–anoxic–oxic (AAO) process of the Panjin wastewater plant, with a phosphate content of 4.0 mg L^{-1} . An amount of 0.1 g Ca-MSBC was weighed and added to 100 mL of actual wastewater, stirred in a constant temperature shaker at 30 r min^{-1} for 10 min, and the content of phosphate in the filtrate was measured after filtration using quantitative filter paper.

3.3.2. Adsorption Performance Index

The phosphate content in the liquid phase was determined according to the national standard (GB 11893-1989) ammonium molybdate spectrophotometric method. The phosphate adsorption capacity was used as an indicator of Ca-MSBC adsorption performance. The equilibrium adsorption capacity (q , mg g^{-1}) of the adsorbent was calculated according to the following Equation (1):

$$q = \frac{(c_0 - c) \times V}{m} \quad (1)$$

where c_0 and c (mg L^{-1}) are the initial and final concentrations of phosphate, V is the volume of solution (L), and m (g) is the mass of Ca-MSBC.

3.3.3. Adsorption Kinetic Model

To further understand the kinetic mechanism of phosphorus adsorption, three commonly used models were used to evaluate the data:

$$\text{Pseudo-first-order : } \ln(q_e - q_t) = \ln q_e - k_1 t \quad (2)$$

$$\text{Pseudo-second-order : } \frac{t}{q_t} = \frac{1}{k_2 q_e^2} + \frac{t}{q_e} \quad (3)$$

$$\text{Intra-particle diffusion : } q_t = k_p t^{0.5} + C_i \quad (4)$$

where q_e (mg g^{-1}) and q_t (mg g^{-1}) are the phosphate adsorption capacity of the adsorbent at equilibrium and time t , respectively, and k_1 (min^{-1}), k_2 ($\text{g mg}^{-1} \text{min}^{-1}$), and k_p [$\text{g} (\text{mg}^{-1} \text{min}^{0.5})^{-1}$] are the adsorption kinetic constants.

3.3.4. Adsorption Thermodynamics

Ca-MSBC was synthesized for phosphate removal from wastewater, where one of the most significant factors affecting phosphate adsorption is temperature. Equations (5)–(7) were used to calculate the relevant thermodynamic parameters, the Gibbs free energy change (ΔG^θ , KJ mol^{-1}), average standard enthalpy (ΔH^θ , KJ mol^{-1}), and standard entropy change (ΔS^θ , $\text{KJ mol}^{-1} \text{K}^{-1}$) to verify the effect of temperature on the adsorption process.

$$K_d = \frac{q_e}{c_e} \quad (5)$$

$$\Delta G = -RT \ln K_d \quad (6)$$

$$\ln K_d = -\frac{\Delta H}{RT} + \frac{\Delta S}{R} \quad (7)$$

where R ($8.314 \text{ J mol}^{-1} \cdot \text{K}^{-1}$) is the universal gas constant, T is the adsorption temperature (K), K_d is the equilibrium constant, which is calculated by plotting $\ln K_d$ versus T^{-1} (Figure S1), q_e is the equilibrium adsorption capacity (mg g^{-1}), and c_e is the equilibrium concentration (mg L^{-1}).

3.4. Analytical Methods

An X-ray diffractometer (XRD) was used to determine the fabricated materials structure and crystalline form (D8 Advance, Bruker, Karlsruhe, Germany), with Cu target as the radiation source with a radiation wavelength of 1.5418 \AA , scanning range of $5\text{--}90^\circ$, an operating voltage of 40 kV, and an operating current of 40 mA. A scanning electron microscope (SEM) (Jsm7610f, JEOL's, Tokyo, Japan) was used to observe the materials' microscopic morphology and surface structure, operating at a voltage of 20 kV.e. A Fourier transform infrared spectrometer (FT-IR) was used to analyze the surface functional groups (WQF-520, Bei Fen Rui Li, Beijing, China) in the range of 4400–400 cm^{-1} . A vibrating sample magnetometer (VSM) was used to measure the magnetization curve that characterizes the material (7407, Lakeshore, Westerville, OH, USA) under an applied magnetic field of ± 2000 Oe. N_2 adsorption/desorption isotherms (ASAP2460, Micromeritics, America) specific surface area, average porosity, and total pore volume of Ca-MSBC were measured using the Quantachrome Instruments N_2 adsorption–desorption method. Elements in Ca-MSBC samples were quantitatively determined by inductively coupled plasma mass spectrometry (ICP-MS) (ICAP7400, ThermoFisher, Waltham, MA, USA). The chemical composition and surface functional groups of the prepared materials were analyzed using

X-ray photoelectron spectroscopy (XPS) (ESCALAB 250Xi, ThermoFisher, Waltham, MA, USA) with Al K α radiation at a voltage of 12 kV and a current of 6 mA. The content of C and O elements in the material was determined by an element analyzer (FlashSmart, ThermoFisher, Waltham, MA, USA).

4. Conclusions

Herein, a sludge-sourced mesoporous Ca-MSBC adsorbent was prepared by a simple and green one-step hydrothermal method for the effective removal of phosphate from real wastewater. Interestingly, Ca-modified Ca-MSBC adsorbent exhibits excellent adsorption performance towards phosphates in alkaline conditions in wastewater, with the main adsorption mechanism being physisorption according to the ΔH^{θ} value and thermodynamics of adsorption. The maximum adsorption capacity of Ca-MSBC for phosphates is 89.25 mg g $^{-1}$, and after nine consecutive adsorption–desorption cycles, Ca-MSBC still retained a high adsorption capacity for phosphates. Additionally, the coexistence of anions such as Cl $^{-}$, NO $_3^{-}$, SO $_4^{2-}$, and CO $_3^{2-}$ has little effect on the adsorption of phosphates by Ca-MSBC. Moreover, Ca-MSBC still has a good adsorption effect on phosphorus in actual wastewater, and the phosphorus content of the adsorbed wastewater meets the national wastewater discharge standard of <0.5 mg L $^{-1}$. To the best of our knowledge, this is the first report on a Ca-modified magnetic sludge biochar adsorbent acting as an excellent phosphate adsorbent. Taking into account its ease of preparation, cost-effectiveness, environmental friendliness, stable performance, and high efficiency, Ca-MSBC has great potential for the high-value utilization of SS.

Supplementary Materials: The following supporting information can be downloaded at: <https://www.mdpi.com/article/10.3390/catal13060927/s1>, Figure S1: Linear plot of $\ln K_d$ vs. $1/T$; Table S1: ICP-MS and elemental quantitative analysis results; Table S2: Specific surface area and pore volume pore size table; Table S3: Comparison of similar feedstock adsorption capacities; Table S4: Thermodynamic parameters of phosphate adsorption on Ca-MSBC.

Author Contributions: Writing—original draft preparation, X.L.; methodology and investigation, Y.L. and H.Z.; validation, formal analysis, C.L.; visualization, B.A.; conceptualization, Y.X.; validation, J.G. and Z.L. All authors have read and agreed to the published version of the manuscript.

Funding: This study was funded by the Liaoning Key Laboratory of Chemical Additive Synthesis and Separation (ZJKF2101, ZJKF2102) and the Anhui Provincial Science and Technology Department Concentric Science and Innovation Project (202206e08020007).

Data Availability Statement: The data presented in this study are available on request from the corresponding author.

Acknowledgments: The authors are grateful to Dawei Wang, Liaoning Huaifu Environmental Engineering Co., Ltd. for providing the actual effluent samples for this study.

Conflicts of Interest: The authors declare no conflict of interest.

References

1. Jellali, S.; Khiari, B.; Usman, M.; Hamdi, H.; Charabi, Y.; Jeguirim, M. Sludge-derived biochars: A review on the influence of synthesis conditions on pollutants removal efficiency from wastewaters. *Renew. Sustain. Energy Rev.* **2021**, *144*, 111068. [[CrossRef](#)]
2. Zhang, Y.; Shi, G.; Wu, W.; Ali, A.; Wang, H.; Wang, Q.; Xu, Z.; Qi, W.; Li, R.; Zhang, Z. Magnetic biochar composite decorated with amino-containing biopolymer for phosphorus recovery from swine wastewater. *Colloids Surf. A Physicochem. Eng. Asp.* **2022**, *634*, 127980. [[CrossRef](#)]
3. Almanassra, I.W.; Mckay, G.; Kochkodan, V.; Atieh, M.A.; Al-Ansari, T. A state of the art review on phosphate removal from water by biochars. *Chem. Eng. J.* **2021**, *409*, 128211. [[CrossRef](#)]
4. Stockman, J.; Villaverde, C.; Corbee, R.J. Calcium, Phosphorus, and Vitamin D in Dogs and Cats. The Veterinary clinics of North America. *Small Anim. Pract.* **2021**, *51*, 623–634. [[CrossRef](#)] [[PubMed](#)]
5. Li, X.; Zhao, X.; Zhou, X.; Yang, B. Phosphate recovery from aqueous solution via struvite crystallization based on electrochemical-decomposition of nature magnesite. *J. Clean. Prod.* **2021**, *292*, 126039. [[CrossRef](#)]
6. Hao, Z.; Zhao, S.; Li, Q.; Wang, Y.; Zhang, J.; Wang, Z.; Wang, J. Reverse osmosis membranes with sulfonate and phosphate groups having excellent anti-scaling and anti-fouling properties. *Desalination* **2021**, *509*, 115076. [[CrossRef](#)]

7. Rashid, S.S.; Liu, Y.; Zhang, C. Upgrading a large and centralised municipal wastewater treatment plant with sequencing batch reactor technology for integrated nutrient removal and phosphorus recovery: Environmental and economic life cycle performance. *Sci. Total Environ.* **2020**, *749*, 141465. [[CrossRef](#)]
8. Liu, W.; Shen, C.; Liu, C.; Zhang, S.; Hao, S.; Peng, Y.; Li, J. Achieving stable mainstream nitrogen and phosphorus removal assisted by hydroxylamine addition in a continuous partial nitrification/anammox process from real sewage. *Sci. Total Environ.* **2021**, *794*, 148478. [[CrossRef](#)]
9. Xiao, Y.; Raheem, A.; Ding, L.; Chen, W.-H.; Chen, X.; Wang, F.; Lin, S.-L. Pretreatment, modification and applications of sewage sludge-derived biochar for resource recovery—A review. *Chemosphere* **2022**, *287*, 131969. [[CrossRef](#)]
10. Di Capua, F.; de Sario, S.; Ferraro, A.; Petrella, A.; Race, M.; Pirozzi, F.; Fratino, U.; Spasiano, D. Phosphorous removal and recovery from urban wastewater: Current practices and new directions. *Sci. Total Environ.* **2022**, *823*, 153750. [[CrossRef](#)]
11. Albatrni, H.; Qiblawey, H.; Al-Marri, M.J. Walnut shell based adsorbents: A review study on preparation, mechanism, and application. *J. Water Process Eng.* **2022**, *45*, 102527. [[CrossRef](#)]
12. Jeyasubramanian, K.; Thangagiri, B.; Sakthivel, A.; Raja, J.D.; Seenivasan, S.; Vallinayagam, P.; Madhavan, D.; Devi, S.M.; Rathika, B. A complete review on biochar: Production, property, multifaceted applications, interaction mechanism and computational approach. *Fuel* **2021**, *292*, 120243. [[CrossRef](#)]
13. Hao, Z.; Wang, C.; Yan, Z.; Jiang, H.; Xu, H. Magnetic particles modification of coconut shell-derived activated carbon and biochar for effective removal of phenol from water. *Chemosphere* **2018**, *211*, 962–969. [[CrossRef](#)] [[PubMed](#)]
14. Santiviago Petzoldt, C.; Peralta Lezcano, J.; López Moreda, I. Removal of orthophosphate and dissolved organic phosphorus from synthetic wastewater in a combined struvite precipitation-adsorption system. *J. Environ. Chem. Eng.* **2020**, *8*, 103923. [[CrossRef](#)]
15. Chen, B.; Chen, Z.; Lv, S. A novel magnetic biochar efficiently sorbs organic pollutants and phosphate. *Bioresour. Technol.* **2011**, *102*, 716–723. [[CrossRef](#)]
16. Rong, X.; Xie, M.; Kong, L.; Natarajan, V.; Ma, L.; Zhan, J. The magnetic biochar derived from banana peels as a persulfate activator for organic contaminants degradation. *Chem. Eng. J.* **2019**, *372*, 294–303. [[CrossRef](#)]
17. Paul, N.J.; Prasanna, K. Utilization of shell-based agricultural waste adsorbents for removing dyes: A review. *Chemosphere* **2022**, *291 Pt 1*, 132737. [[CrossRef](#)]
18. Zhang, S.; Ji, Y.; Dang, J.; Zhao, J.; Chen, S. Magnetic apple pomace biochar: Simple preparation, characterization, and application for enriching Ag(I) in effluents. *Sci. Total Environ.* **2019**, *668*, 115–123. [[CrossRef](#)]
19. Álvarez, M.; Gascó, G.; Palacios, T.; Paz-Ferreiro, J.; Méndez, A. Fe oxides-biochar composites produced by hydrothermal carbonization and pyrolysis of biomass waste. *J. Anal. Appl. Pyrolysis* **2020**, *151*, 104893. [[CrossRef](#)]
20. Cao, H.; Wu, X.; Syed-Hassan, S.S.A.; Zhang, S.; Mood, S.H.; Milan, Y.J.; Garcia-Perez, M. Characteristics and mechanisms of phosphorous adsorption by rape straw-derived biochar functionalized with calcium from eggshell. *Bioresour. Technol.* **2020**, *318*, 124063. [[CrossRef](#)] [[PubMed](#)]
21. Yang, Z.; Zhu, T.; Xiong, M.; Sun, A.; Xu, Y.; Wu, Y.; Shu, W.; Xu, Z. Tuning adsorption capacity of metal–organic frameworks with Al³⁺ for phosphorus removal: Kinetics, isotherm and regeneration. *Inorg. Chem. Commun.* **2021**, *132*, 108804. [[CrossRef](#)]
22. Rizwan, M.; Lin, Q.; Chen, X.; Li, Y.; Li, G.; Zhao, X.; Tian, Y. Synthesis, characterization and application of magnetic and acid modified biochars following alkaline pretreatment of rice and cotton straws. *Sci. Total Environ.* **2020**, *714*, 136532. [[CrossRef](#)] [[PubMed](#)]
23. Pan, X.; Gu, Z.; Chen, W.; Li, Q. Preparation of biochar and biochar composites and their application in a Fenton-like process for wastewater decontamination: A review. *Sci. Total Environ.* **2021**, *754*, 142104. [[CrossRef](#)]
24. Jung, K.; Lee, S.; Lee, Y.J. Synthesis of novel magnesium ferrite (MgFe₂O₄)/biochar magnetic composites and its adsorption behavior for phosphate in aqueous solutions. *Bioresour. Technol.* **2017**, *245*, 751–759. [[CrossRef](#)] [[PubMed](#)]
25. Wang, J.; Liao, Z.; Ifthikar, J.; Shi, L.; Chen, Z.; Chen, Z. One-step preparation and application of magnetic sludge-derived biochar on acid orange 7 removal via both adsorption and persulfate based oxidation. *RSC Adv.* **2017**, *7*, 11876–18696. [[CrossRef](#)]
26. Zhang, H.; Xue, G.; Chen, H.; Li, X. Magnetic biochar catalyst derived from biological sludge and ferric sludge using hydrothermal carbonization: Preparation, characterization and its circulation in Fenton process for dyeing wastewater treatment. *Chemosphere* **2018**, *191*, 64–71. [[CrossRef](#)]
27. Tang, L.; Yu, J.; Pang, Y.; Zeng, G.; Deng, Y.; Wang, J.; Ren, X.; Ye, S.; Peng, B.; Feng, H. Sustainable efficient adsorbent: Alkali-acid modified magnetic biochar derived from sewage sludge for aqueous organic contaminant removal. *Chem. Eng. J.* **2018**, *336*, 160–169. [[CrossRef](#)]
28. Huang, X.; Wei, D.; Zhang, X.; Fan, D.; Sun, X.; Du, B.; Wei, Q. Synthesis of amino-functionalized magnetic aerobic granular sludge-biochar for Pb(II) removal: Adsorption performance and mechanism studies. *Sci. Total Environ.* **2019**, *685*, 681–689. [[CrossRef](#)]
29. Peng, G.; Jiang, S.; Wang, Y.; Zhang, Q.; Cao, Y.; Sun, Y.; Zhang, W.; Wang, L. Synthesis of Mn/Al double oxygen biochar from dewatered sludge for enhancing phosphate removal. *J. Clean. Prod.* **2020**, *251*, 119725. [[CrossRef](#)]
30. Zhang, L.; Liu, J.; Guo, X. Investigation on mechanism of phosphate removal on carbonized sludge adsorbent. *J. Environ. Sci.* **2018**, *64*, 335–344. [[CrossRef](#)]
31. Yoon, K.; Cho, D.-W.; Tsang, D.C.; Bolan, N.; Rinklebe, J.; Song, H. Fabrication of engineered biochar from paper mill sludge and its application into removal of arsenic and cadmium in acidic water. *Bioresour. Technol.* **2017**, *246*, 69–75. [[CrossRef](#)]

32. Wang, Z.; Miao, R.; Ning, P.; He, L. From wastes to functions: A paper mill sludge-based calcium-containing porous biochar adsorbent for phosphorus removal. *J. Colloid Interface Sci.* **2021**, *593*, 434–446. [[CrossRef](#)]
33. Faghihian, M.A.H. Magnetization and functionalization of activated carbon prepared by oak shell biowaste for removal of Pb²⁺ from aqueous solutions. *Chem. Eng. Commun.* **2017**, *205*, 519–532.
34. Jiao, G.-J.; Ma, J.; Li, Y.; Jin, D.; Guo, Y.; Zhou, J.; Sun, R. Enhanced adsorption activity for phosphate removal by functional lignin-derived carbon-based adsorbent: Optimization, performance and evaluation. *Sci. Total Environ.* **2021**, *761*, 143217. [[CrossRef](#)]
35. Huang, C.; Zhang, H.; Zheng, K.; Zhang, Z.; Jiang, Q.; Li, J. Two-dimensional hydrophilic ZIF-L as a highly-selective adsorbent for rapid phosphate removal from wastewater. *Sci. Total Environ.* **2021**, *785*, 147382. [[CrossRef](#)]
36. Du, C.; Song, Y.H.; Shi, S.N.; Jiang, B.; Yang, J.Q.; Xiao, S.H. Preparation and characterization of a novel Fe₃O₄-graphene-biochar composite for crystal violet adsorption. *Sci. Total Environ.* **2020**, *711*, 134662. [[CrossRef](#)]
37. Sung, H.W.F.; Rudowicz, C. Physics behind the magnetic hysteresis loop—A survey of misconceptions in magnetism literature. *J. Magn. Magn. Mater.* **2003**, *260*, 250–260. [[CrossRef](#)]
38. Nascimento, V.X.; Pinto, D.; Lütke, S.F.; da Silva, M.C.F.; Machado, F.M.; Lima, É.C.; Silva, L.F.O. Brilliant blue FCF dye adsorption using magnetic activated carbon from Sapelli wood sawdust. *Environ. Sci. Pollut. Res.* **2023**, *30*, 58684–58696. [[CrossRef](#)]
39. Li, M.; Liu, H.; Chen, T.; Dong, C.; Sun, Y. Synthesis of magnetic biochar composites for enhanced uranium(VI) adsorption. *Sci. Total Environ.* **2019**, *651*, 1020–1028. [[CrossRef](#)]
40. Cychosz, K.A.; Guillet-Nicolas, R.; García-Martínez, J.; Thommes, M. Recent advances in the textural characterization of hierarchically structured nanoporous materials. *Chem. Soc. Rev.* **2017**, *46*, 389–414. [[CrossRef](#)] [[PubMed](#)]
41. Li, X.; Xie, Y.; Jiang, F.; Wang, B.; Hu, Q.; Tang, Y.; Luo, T.; Wu, T. Enhanced phosphate removal from aqueous solution using resourceable nano-CaO₂/BC composite: Behaviors and mechanisms. *Sci. Total Environ.* **2020**, *709*, 136123. [[CrossRef](#)] [[PubMed](#)]
42. Nguyen, V.-T.; Vo, T.-D.; Nguyen, T.-B.; Dat, N.D.; Huu, B.T.; Nguyen, X.-C.; Tran, T.; Le, T.-N.; Duong, T.-G.; Bui, M.-H.; et al. Adsorption of norfloxacin from aqueous solution on biochar derived from spent coffee ground: Master variables and response surface method optimized adsorption process. *Chemosphere* **2022**, *288*, 132577. [[CrossRef](#)] [[PubMed](#)]
43. Shen, X.; Liu, Y.; Xu, J.; Dong, H. Removal of phosphorus from aqueous solution by natural calcite. *Chin. J. Environ. Eng.* **2010**, *4*, 2461–2465.
44. Khan, M.D.; Chottitupawong, T.; Vu, H.H.T.; Ahn, J.W.; Kim, G.M. Removal of Phosphorus from an Aqueous Solution by Nanocalcium Hydroxide Derived from Waste Bivalve Seashells: Mechanism and Kinetics. *ACS Omega* **2020**, *5*, 12290–12301. [[CrossRef](#)] [[PubMed](#)]
45. Mitrogiannis, D.; Psychoyou, M.; Baziotis, I.; Inglezakis, V.J.; Koukouzas, N.; Tsoukalas, N.; Palles, D.; Kamitsos, E.; Oikonomou, G.; Markou, G. Removal of phosphate from aqueous solutions by adsorption onto Ca(OH)₂ treated natural clinoptilolite. *Chem. Eng. J.* **2017**, *320*, 510–522. [[CrossRef](#)]
46. Zou, Y.; Zhang, R.; Wang, L.; Xue, K.; Chen, J. Strong adsorption of phosphate from aqueous solution by zirconium-loaded Ca-montmorillonite. *Appl. Clay Sci.* **2020**, *192*, 105638. [[CrossRef](#)]
47. Zhang, M.; Lin, K.; Li, X.; Wu, L.; Yu, J.; Cao, S.; Zhang, D.; Xu, L.; Parikh, S.J.; Ok, Y.S. Removal of phosphate from water by paper mill sludge biochar. *Environ. Pollut.* **2022**, *293*, 118521. [[CrossRef](#)]
48. Park, J.H.; Ok, Y.S.; Kim, S.H.; Cho, J.S.; Heo, J.S.; Delaune, R.D.; Seo, D.C. Evaluation of phosphorus adsorption capacity of sesame straw biochar on aqueous solution: Influence of activation methods and pyrolysis temperatures. *Env. Geochem. Health* **2015**, *37*, 969–983. [[CrossRef](#)]
49. Fang, C.; Zhang, T.; Li, P.; Jiang, R.F.; Wang, Y.C. Application of magnesium modified corn biochar for phosphorus removal and recovery from swine wastewater. *Int. J. Environ. Res. Public Health* **2014**, *11*, 9217–9237. [[CrossRef](#)]
50. Zhang, M.; Gao, B.; Fang, J.; Creamer, A.E.; Ullman, J.L. Self-assembly of needle-like layered double hydroxide (LDH) nanocrystals on hydrochar: Characterization and phosphate removal ability. *RSC Adv.* **2014**, *4*, 28171–28175. [[CrossRef](#)]
51. Ahmed, M.; Aziziha, M.; Anwar, R.; Johnson, M.B.; Lin, L.-S. Magnetic sludge byproducts for adsorptive phosphorus removal: Resource recovery from iron-based anaerobic sewage sludge. *Waste Manag.* **2021**, *120*, 269–276. [[CrossRef](#)]
52. Dong, X.; Ma, L.Q.; Zhu, Y.; Li, Y.; Gu, B. Mechanistic Investigation of Mercury Sorption by Brazilian Pepper Biochars of Different Pyrolytic Temperatures Based on X-ray Photoelectron Spectroscopy and Flow Calorimetry. *Environ. Sci. Technol.* **2013**, *47*, 12156–12164. [[CrossRef](#)]
53. Liu, R.; Chi, L.; Wang, X.; Sui, Y.; Wang, Y.; Arandiyán, H. Review of metal (hydr)oxide and other adsorptive materials for phosphate removal from water. *J. Environ. Chem. Eng.* **2018**, *6*, 5269–5286. [[CrossRef](#)]
54. Mekonnen, D.T.; Alemayehu, E.; Lennartz, B. Removal of Phosphate Ions from Aqueous Solutions by Adsorption onto Leftover Coal. *Water* **2020**, *12*, 1381. [[CrossRef](#)]
55. Lima, E.C.; Hosseini-Bandegharaei, A.; Moreno-Piraján, J.C.; Anastopoulos, I. A critical review of the estimation of the thermodynamic parameters on adsorption equilibria. Wrong use of equilibrium constant in the Van't Hoff equation for calculation of thermodynamic parameters of adsorption. *J. Mol. Liq.* **2019**, *273*, 425–434. [[CrossRef](#)]
56. Ho, Y.S. Removal of copper ions from aqueous solution by tree fern. *Water Res.* **2003**, *37*, 2323–2330. [[CrossRef](#)]
57. Wang, B.; Zhang, W.; Li, L.; Guo, W.; Xing, J.; Wang, H.; Hu, X.; Lyu, W.; Chen, R.; Song, J.; et al. Novel talc encapsulated lanthanum alginate hydrogel for efficient phosphate adsorption and fixation. *Chemosphere* **2020**, *256*, 127124. [[CrossRef](#)]

58. He, J.; Xu, Y.; Wang, W.; Hu, B.; Wang, Z.; Yang, X.; Wang, Y.; Yang, L. Ce(III) nanocomposites by partial thermal decomposition of Ce-MOF for effective phosphate adsorption in a wide pH range. *Chem. Eng. J.* **2020**, *379*, 122431. [[CrossRef](#)]
59. Liu, M.; Li, S.; Tang, N.; Wang, Y.; Yang, X.; Wang, S. Highly efficient capture of phosphate from water via cerium-doped metal-organic frameworks. *Clean. Prod. J.* **2020**, *265*, 121782. [[CrossRef](#)]
60. Wang, J.; Xia, Y. Fe-Substituted Isorecticular Metal–Organic Framework for Efficient and Rapid Removal of Phosphate. *ACS Appl. Nano Mater.* **2019**, *2*, 6492–6502. [[CrossRef](#)]
61. Mäkelä, M.; Yoshikawa, K. Simulating hydrothermal treatment of sludge within a pulp and paper mill. *Appl. Energy* **2016**, *173*, 177–183. [[CrossRef](#)]

Disclaimer/Publisher’s Note: The statements, opinions and data contained in all publications are solely those of the individual author(s) and contributor(s) and not of MDPI and/or the editor(s). MDPI and/or the editor(s) disclaim responsibility for any injury to people or property resulting from any ideas, methods, instructions or products referred to in the content.